J Therm Anal Calorim (2012) 108:951–958
DOI 10.1007/s10973-012-2385-4

Effect of magnesium doping on the properties and crystalline perfection of bis(thiourea)zinc(II) chloride crystals

K. Muthu · G. Bhagavannarayana · V. Meenatchi · S. P. Meenakshisundaram · S. C. Mojumdar

CTAS2011 Conference Special Chapter

Abstract In this article, the effect of magnesium doping on the properties of bis(thiourea)zinc(II) chloride (BTZC) crystals has been described. The incorporation of Mg(II) into the crystal lattice was confirmed by energy dispersive X-ray spectroscopy and quantified by inductively coupled plasma technique. The powder X-ray diffraction and FT-IR spectral analyses indicate that the crystal undergoes considerable stress as result of doping. SEM studies of pure and doped samples indicate the formation of structural defect centers in BTZC crystals. The TG–DTA studies reveal the purity of the materials, and no decomposition is observed up to the melting point. Improved crystalline perfection by doping is observed by high-resolution X-ray diffraction. High transmittance is observed, and the cutoff λ is $\sim$295 nm.

Keywords Mg-doping · HRXRD · ICP analysis · TG–DTA · SEM

K. Muthu · V. Meenatchi · S. P. Meenakshisundaram
Department of Chemistry, Annamalai University, Annamalainagar 608 002, India

G. Bhagavannarayana
Materials Characterization Division, National Physical Laboratory, New Delhi 110 012, India

S. C. Mojumdar (✉)
Department of Chemical Technologies and Environment, Faculty of Industrial Technologies, Trenčín University of A. Dubček, 020 32 Púchov, Slovakia
e-mail: scmojumdar@yahoo.com

S. C. Mojumdar
Department of Chemistry, University of Guelph, Guelph, ON, Canada

Introduction

The semiorganic crystals are used as new frequency generators, because of their high resistance to laser-induced damage, low angular sensitivity, and good mechanical hardness [1–8]. Among the semiorganic materials, metal complexes of thiourea which have low ultraviolet (UV) cutoff wavelengths, applicable for high power frequency conversion, have received much attention [9]. Bis(thiourea)zinc(II) chloride (BTZC) is a semi-organic nonlinear optical (NLO) material which finds applications in the area of laser technology, optical communication, data storage technology, optical computing, etc., Metal ion-doped materials are currently receiving a great deal of attention because of the rapid development of laser diodes [10, 11]. Several foreign metallic cations existing in the parent compounds with high valency and small radii will affect the whole growth process and enhances physical properties. Their effects are related with ionic radius, electric charge, and frequency of solvent exchange [12–14]. The crystal growth, pH effects, kinetics and doping effects on BTZC have been extensively studied [15–25].

Incorporation of Mg into pure a-$LiIO_3$ [26] and BTCC [27, 28] crystals significantly enhances the electrical conductivity, microhardness and the dielectric properties. Ultraviolet one-color photo refraction (UV-OPR) is enhanced by Mg doping [29]. The second harmonic generation (SHG) conversion efficiency was enhanced by the presence of Mg in $LiNbO_3$ crystals. The optical damage, which is a serious problem with $LiNbO_3$ crystals, can be reduced by doping with Mg [30]. The Mg concentration in Mg-doped $(Ba_{0.6}Sr_{0.4})_{0.92}K_{0.075}TiO_3$ thin films has a strong influence on the materials' properties including surface morphology, dielectric and tunable properties [31].These aspects prompted us to use Mg as a dopant material in the technologically

important BTZC crystals. Thermal, X-ray and spectral analyses are very useful techniques for materials characterization. Therefore, many authors have applied these methods for various materials characterization [32–52]. In the present work, attempts have been made to improve the physico-chemical properties by incorporating alkaline earth metal as dopant.

Experimental

Synthesis and crystal growth

Bis(thiourea)zinc(II) chloride was synthesized using AR grade zinc chloride and thiourea in a stoichiometric ratio of 1:2 and the chemical reaction is given as

$$ZnCl_2 + 2\left(SC(NH_2)_2\right) \rightarrow [Zn\left(SC(NH_2)_2\right)_2]Cl_2$$

The synthesized (BTZC) material was further purified by recrystallization process using de-ionized water as solvent. Crystals were grown by slow evaporation solution growth technique. Doping with magnesium (1 and 10 mol%) in the form of magnesium chloride was done during the crystallization process. The crystallization took place within 15–20 days, and the crystals were harvested when they attained an optimal size and shape. Photographs of the as-grown pure and doped crystals are shown in Fig. 1.

Characterization studies

Powder XRD analysis was performed on a Philips Xpert Pro Triple-axis X-ray diffractometer at room temperature using a wavelength of 1.540 Å and a step size of 0.008°. The samples were examined with CuK_α radiation in a 2θ range of 10 to 70°. The XRD data were analyzed by Rietveld method with RIETAN-2000. Bruker AXS (Kappa Apex II) X-ray diffractometer was used for single crystal XRD studies. A multicrystal XRD developed at NPL [53] has been used to record high-resolution diffraction curves (DCs). Fourier transform infrared spectra were recorded on an AVATAR 330 FT-IR spectrometer. UV–Vis spectra were recorded on a CARY 5E UV–Vis–NIR spectrophotometer. The surface morphology was observed on a JEOL JSM 5610 LV scanning electron microscope. Simultaneous TG–DTA curves were recorded on a SDT Q600 (TA instrument) thermal analyzer. The TG–DTA curves were simultaneously obtained in nitrogen at a heating rate of 10 °C min^{-1}. ICP studies were recorded on an Optima 5000 DV series spectrometer.

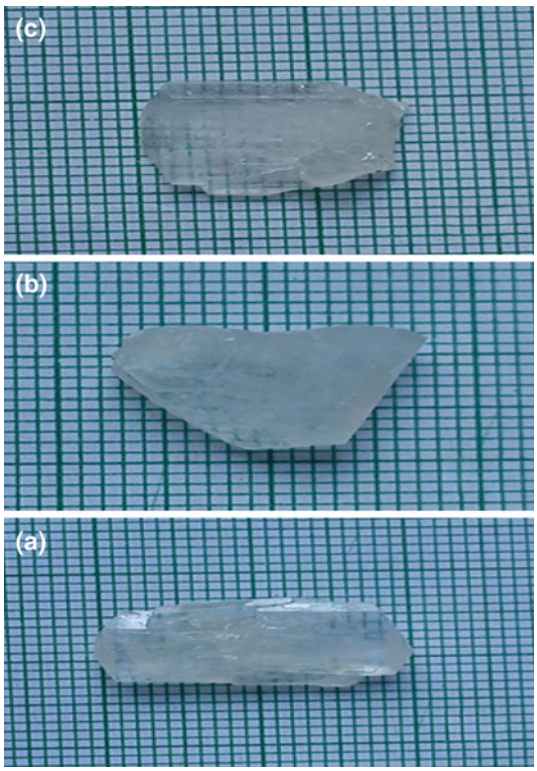

Fig. 1 Photographs of as-grown BTZC crystals: **a** pure, **b** 1 mol% Mg-doped and **c** 10 mol% Mg-doped

Table 1 Values of lattice constants a (Å), b (Å), c (Å) and cell volume V $(Å)^3$

Property	Pure BTZC[a]	Doped BTZC (~10 mol%)
a	13.012	13.04
b	12.768	12.76
c	5.890	5.90
V	978.64	981

[a] Ref. [16]

Results and discussion

Single crystal X-ray analysis

To determine the unit cell parameters the as-grown crystals were subjected to single crystal X-ray diffraction studies using Bruker AXS (Kappa Apex II) X-ray diffractometer. Single crystal XRD data were collected on a diffraction system which employs graphite monochromated MoKα radiation ($\lambda =$ 0.71073 Å). The as-grown crystal belongs to orthorhombic system with space group Pnma, and the cell parameters of pure and doped BTZC crystals are given in Table 1.

Powder X-ray diffraction analysis

The powder XRD pattern of doped BTZC is compared with undoped one (Fig. 2). The XRD profiles show that the samples were of single phase without detectable impurity. No change in the basic structure is observed except for the slight reduction in intensity with alkaline earth metal doping. These observations could be due to lattice strain on account of doping.

High-resolution X-ray diffraction analysis

To reveal the crystalline perfection of the as-grown crystals and to study the effect of dopant, a multicrystal X-ray diffractometer developed at NPL was used to record high-resolution diffraction curves (DCs). In this system, a fine-focus (0.4 × 8 mm; 2 kW Mo) X-ray source energized by a well-stabilized Philips X-ray generator (PW 1743) is employed. The well-collimated and monochromated MoKα_1 beam obtained from the three monochromator Si crystals set in dispersive (+, −, −) configuration is used as the exploring X-ray beam. This arrangement improves the spectral purity ($\Delta\lambda/\lambda 10^{-5}$) of the MoK$\alpha_1$ beam. The divergence of the exploring beam in the horizontal plane (plane of diffraction) is estimated to be $\ll$3 arc s. The specimen crystal is aligned in the (+, −, −, +) configuration. Owing to the dispersive configuration, though the lattice constant of the monochromator crystal(s) and the specimen are different, the unwanted dispersion broadening in the diffraction curve of the specimen crystal is insignificant. The specimen can be rotated about a vertical axis, which is perpendicular to the plane of diffraction, with minimum angular interval of 0.5 arc s. The diffracted intensity is measured by using a scintillation counter.

Figure 3a shows the high-resolution diffraction curve (DC) recorded for a typical BTZC single crystal specimen using (200) diffracting planes in symmetrical Bragg geometry. The solid line (convoluted curve) is well fitted with the experimental points represented by the filled circles. On deconvolution of the diffraction curve, it is clear that the curve contains two additional peaks, which are 1,018 and 168 arc s away from the main peak. These two additional peaks correspond to two internal structural low angle boundaries tilt angles of which are 1,018 and 168 arc s from the main crystal block. The full width at half maximum (FWHM) of the main peak and the low angle boundaries are respectively 344 and 730 and 44 arc s. Though the specimen contains low angle boundaries, the relatively low angular spread of around 2,000 arc s (around half a degree) of the diffraction curve and the low FWHM values show that the crystalline perfection is reasonably good. The effect of such very low angle boundaries may not be very significant in many device applications; however. for applications like phase matching, it is better to know these minute details regarding crystalline perfection.

Figure 3b shows the high-resolution diffraction curve (DC) recorded for Mg^{2+}-doped specimen. As seen in the Fig. 3b, the DC contains a single peak and indicates that the specimen is free from structural grain boundaries. The

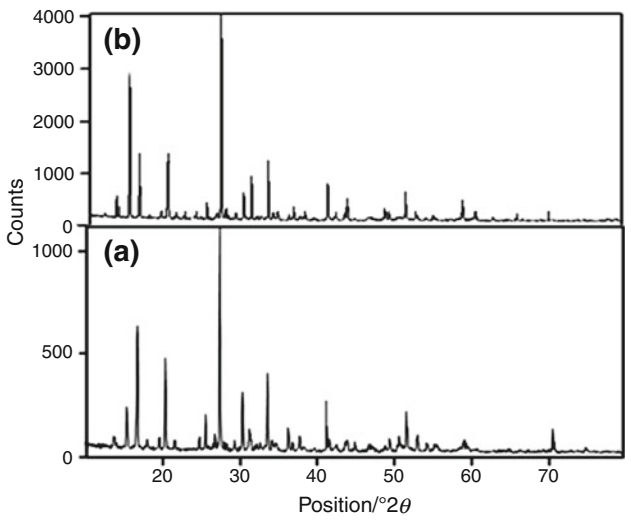

Fig. 2 Powder XRD patterns of BTZC crystals: **a** pure and **b** 10 mol% Mg-doped

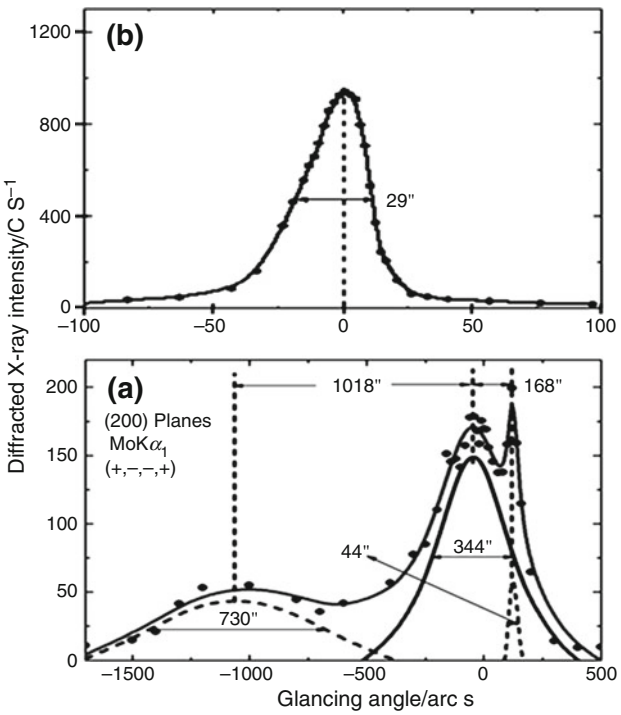

Fig. 3 HRXRD curves recorded for **a** pure BTZC and **b** 10 mol% Mg-doped BTZC

FWHM of this curve is 29 arc s which is somewhat more than that expected from the plane wave theory of dynamic X-ray diffraction [54], for an ideally perfect crystal but close to that expected for nearly perfect real-life crystals. This much broadness with good scattered intensity along the wings of the DC indicates that the crystal contains point defects and their aggregates. Such defects are very common to observe in almost all real-life crystals including nature-gifted crystals and are many times unavoidable because of thermodynamic conditions.

It is interesting to see the shape of the DC. As seen in the figure, the DC is not symmetric with respect to the Bragg peak position, which indicates that the density of vacancy and interstitial defects are not same. For a particular angular deviation ($\Delta\theta$) of glancing angle (θ) with respect to the Bragg peak position (taken as zero for the sake of convenience), the scattered intensity is much more in the negative direction in comparison to that of the positive direction. This feature clearly indicates that the crystal contains predominantly vacancy type of defects than that of interstitial defects. This can be well understood by the fact that because of vacancy defects (which may arise because of fast growth or incorporation of impurities of lesser size at the substitutional sites or because of antisitic defects due to incorporation of dopants with different valances to that of the host ions), the lattice around these defects undergo tensile stress, and the lattice parameter d (interplanar spacing) increases and leads to result in more scattered (also known as diffuse X-ray scattering) intensity at slightly lower Bragg angles (θ_B), as d and sin θ_B are inversely proportional to each other in the Bragg equation ($2d$ sin $\theta_B = n\lambda$; n and λ are the orders of reflection and wavelength, respectively, which are fixed). The inset in the curve shows the schematic to illustrate how the lattice around the defect core undergoes tensile stress. The converse explanation is true in case of interstitial defects which cause compressive stress in the lattice around the defect core leading to decrease of lattice spacing and, in turn, results in more scattered intensity at the higher Bragg angles. However, the single diffraction curve with reasonably low FWHM indicates that the crystalline perfection is fairly good. The density of such vacancy defects is, however, meager, and in almost all real crystals including nature-gifted crystals, such defects are commonly observed and are many times unavoidable because of thermodynamical conditions, and they hardly affect the device performance. More details may be obtained from the study of high-resolution diffuse X-ray scattering measurements [53], which is, however, not the main focus of the present investigation. It is worth mentioning here that the observed scattering due to point defects is of short-range order as the strain due to such minute defects is limited to the very defect core and the long-range order could not be expected, and hence the change in the lattice parameter of the overall crystal is not expected. It may be mentioned here that the minute information like the asymmetry in the DC could be possible as in the present sample, only because of the high-resolution of the multicrystal X-ray diffractometer used in the present investigation.

FT-IR spectral analysis

The FT-IR spectra of pure and doped crystals reveal that the characteristic vibrational patterns of pure and doped BTZC are very close to each other (Fig. 4). Small shifts in some of the characteristic vibrational frequencies are observed. It could be due to lattice strain as a result of metal doping. The symmetric and asymmetric C=S stretching vibrations, respectively, at 740 and 1,417 cm^{-1} of thiourea are shifted to lower frequencies ($\sim$716 and $\sim$1,406 cm^{-1}, respectively) in the FT-IR spectra of pure and doped BTZC crystals. The N–C–N stretching frequencies of thiourea (1,089 and 1,472 cm^{-1}, respectively) are shifted to higher frequencies for pure and magnesium-doped BTZC crystals ($\sim$1,103 and $\sim$1,496 cm^{-1}, respectively). These observations suggest that metals coordinate with thiourea through sulfur atom.

Optical transmission spectral analysis

The UV–Visible spectra were recorded for the doped and undoped BTZC crystals. It is observed that doping does not altere the optical transmission (Fig. 5). At the longer wavelength side, the crystal is highly transparent, and it could

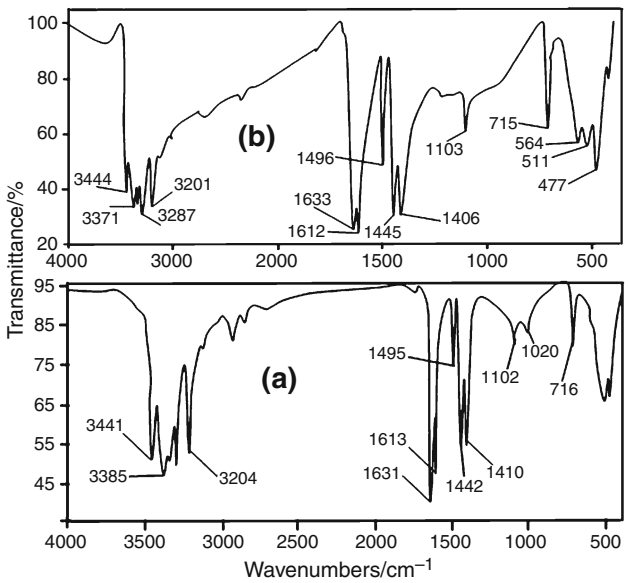

Fig. 4 FT-IR spectrum of BTZC crystals: **a** pure and **b** 10 mol% Mg-doped

be used for optical window applications. The lower cut-off wavelength is ~295 nm.

SEM and EDS analyses

The SEM images were taken at magnification values from 50× to 5,000× with maximum values 20.00 kV on a JEOL JSM 5610 LV scanning electron microscope. It gives information about surface morphology. Also, it is used to check the presence of imperfections. The effect of the influence of dopant on the surface morphology of BTZC crystal faces reveals structure defect centers as shown in the SEM images (Fig. 6). The flower-like morphology of undoped specimen is disturbed to form plate-like morphology by the incorporation of Mg^{2+} in the crystalline matrix.

Incorporation of Mg(II) dopant into the crystalline matrix was observed by EDS (Fig. 7). It shows that the accommodating capability of the host crystal is limited, and only a small quantity is incorporated into the crystalline matrix.

Thermal analysis

The simultaneous TG–DTA curves in nitrogen for pure and doped BTZC systems heated from 30 to 800 °C at a heating rate of 20 °C/min are given in the Fig. 8. The TG–DTA curves appear nearly similar for the two samples with three stages of decomposition between 200 and 800 °C. The absence of water of crystallization in the molecular structure is indicated by the absence of mass loss around

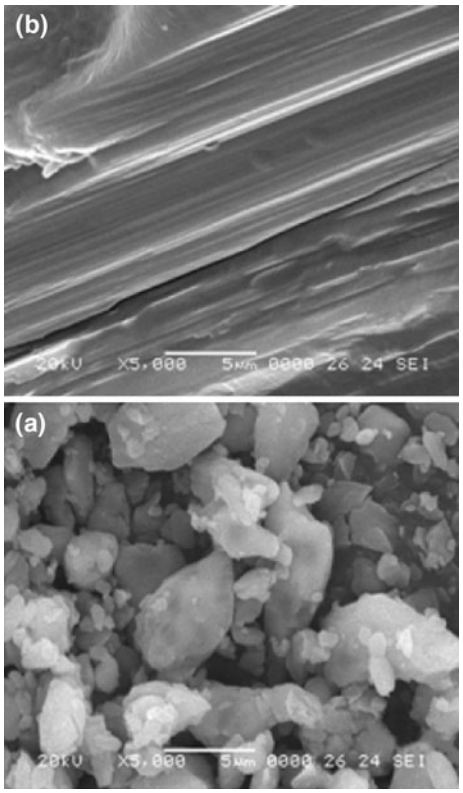

Fig. 6 SEM micrographs of BTZC crystals: **a** pure and **b** 10 mol% Mg-doped

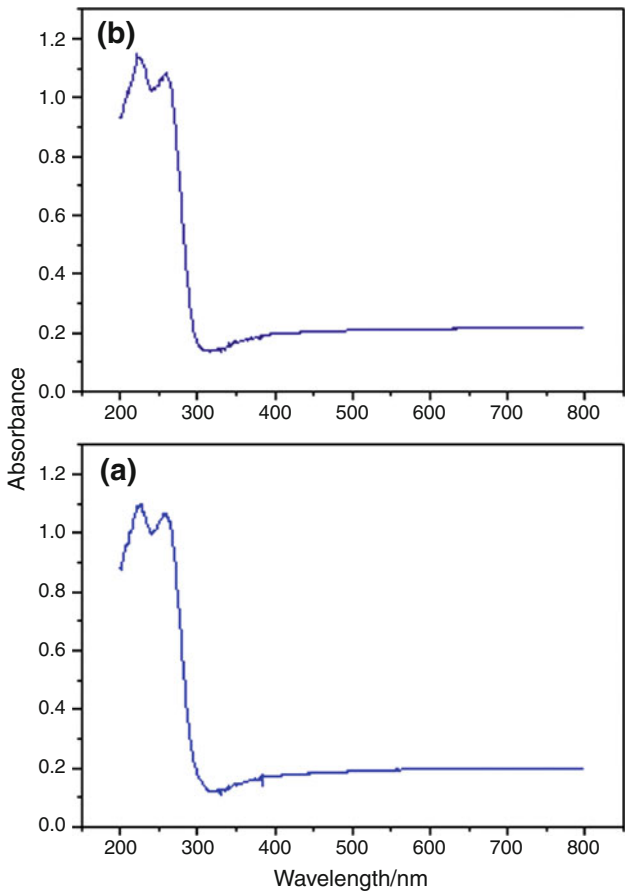

Fig. 5 UV-Vis spectrum of **a** pure and **b** 10 mol% Mg-doped BTZC

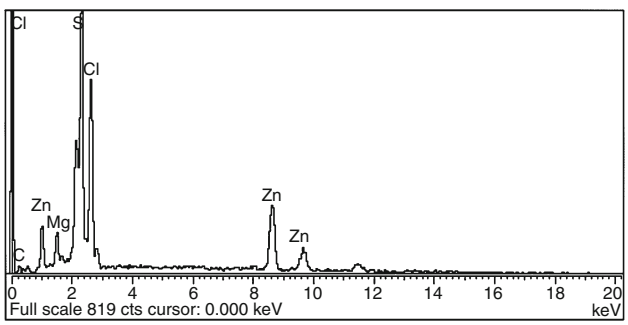

Fig. 7 EDS spectrum of 10 mol% Mg-doped BTZC

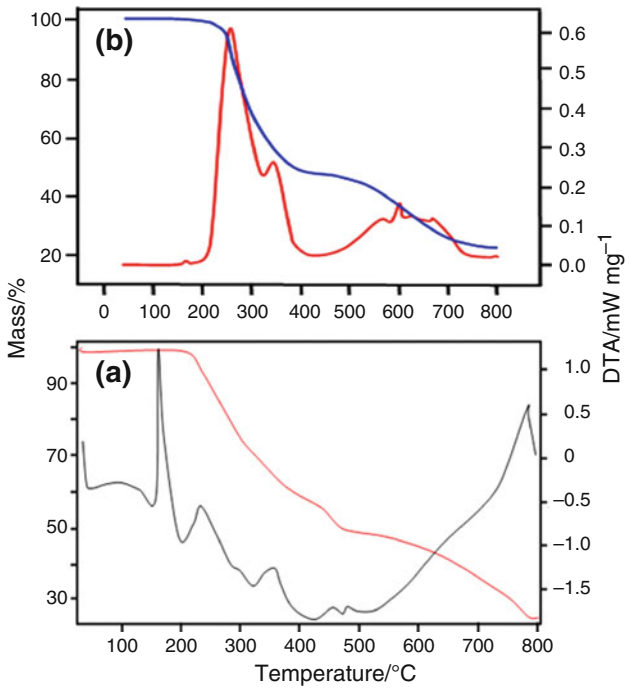

Fig. 8 TG–DTA curves of BTZC crystals: **a** pure and **b** Mg-doped

100 °C. The melting point of the sample is slightly increased in the case of magnesium-added BTZC crystal (Fig. 8b). The slight increment in temperature is evident for doped crystals, suggesting that the incorporation of Mg^{2+} can enhance the thermal stability of the BTZC crystal. The increment in temperature for the doped crystals correlates with the lesser ionic radius of Mg^{2+} (0.65 Å) than that of Zn (0.69 Å). The lesser ionic radius of Mg^{2+} can give more bonding interaction with thiourea, thus giving more thermal stability to the crystal [55]. No decomposition up to the melting point ensures the suitability of the material for application in lasers where the crystals are required to withstand high temperatures.

CP analysis

ICP studies were recorded on an Optima 5000 DV series spectrometer. The amount of Mg^{2+}-dopant in BTZC specimens are estimated using inductive coupled plasma (ICP) technique, and the actual dopant concentration in the crystalline matrices were found to be 0.009 and 0.017 ppm for ~1 and ~10 mol% Mg^{2+}-doped specimens, respectively. The foreign metal ion entering into the BTZC crystal matrix is small but significant. Further, the final dopant concentration within the host lattice is not proportional to the concentration of the crystallization process since the host crystal can accommodate the dopant only to a limited extent.

Conclusions

Single crystals of pure and Mg^{2+}-doped BTZC crystals are grown by slow evaporation solution growth technique at room temperature. A close observation of XRD and FT-IR profiles of doped and undoped specimens reveals strain. SEM images reveal that the external morphology of BTZC crystal is changed by doping. The incorporation of dopant into the crystalline matrix is further established by EDS and ICP analyses. The presence of dopants has marginally altered the lattice parameters without affecting the basic structure of crystals. The optical spectral study reveals that the incorporation of small quantities of dopant does not destroy the optical transmission.

Acknowledgements One of the authors, K. Muthu, is thankful to the CSIR, New Delhi, for the award of a Senior Research Fellowship.

References

1. Zhang N, Jiang MH, Yuan DR, Xu D, Tao XT, Shao ZS. The quality and performance of the organometallic complex nonlinear optical material tri-allylthiourea cadmium chloride (ATCC). J Cryst Growth. 1990;102:581–4.
2. Ramabadron UB, Zelmon DE, Kennedy GC. Electro-optic, piezoelectric, and dielectric properties of zinc tris thiourea sulfate. Appl Phys Lett. 1992;60:2589–91.
3. Kotler Z, Hierle R, Josse D, Zyss J, Masse R. Quadratic nonlinear-optical properties of a new transparent and highly efficient organic–inorganic crystal: 2-amino-5-nitropyridiniumdihydrogen phosphate (2A5NPDP). J Opt Soc Am B. 1992;9:534–47.
4. Horiuchi N, Lefaucheux F, Ibanez A, Josse D, Zyss J. An organic–inorganic crystal for blue SHG: crystal growth and quadratic optical effect of 2-amino-5-nitropyridinium chloride. Opt Mater. 1999;12:351–6.
5. Narayan Bhat M, Dharmaprakash SM. Growth of nonlinear optical γ-glycine crystals. J Cryst Growth. 2002;236:376–80.
6. Venkataramanan V, Subramanian CK, Bhat HL. Laser induced damage in zinc tris(thiourea) sulfate and bis(thiourea) cadmium chloride. J Appl Phys. 1995;77:6049–51.
7. Warren LF. Electronic materials-our future. In: Allred RE, Martinez RJ, Wischmann KB, editors. Proceedings of the fourth international sample electronics conference, vol. 4. Covina: Society for the Advancement of Material and Process Engineering; 1990. p. 388.
8. Wang WS, Sutter K, Bosshard CH, Pan Z, Arend H, Gunter P, Chapius G, Nicolo F. Optical second-harmonic generation in single crystals of thiosemicarbazide cadmium bromide hydrate ($Cd(NH_2NHCSNH_2)Br_2 \cdot H_2O$). Jpn J Appl Phys. 1988;27:1138–41.
9. Velsko S. Laser program annual report, Lawrence UCRI-JC, 105000. Livermore: Lawrence Livermore National Laboratory; 1990.
10. Long X, Wang G, Han TPJ. Growth and spectroscopic properties of Cr^{3+}-doped $LaSc_3(BO_3)_4$. J Cryst Growth. 2003;249:191–4.
11. Ramajothi J, Dhanuskodi S. Optical and microhardness studies of semiorganic nonlinear optical material: L-histidine tetrafluoroborate. Cryst Res Technol. 2003;38:986–91.
12. Ohachi T, Hamanada M, Konda H, Hayashi D, Taniguchi I, Hashimoto T, Kotani Y. Electrical nucleation and growth of $NaCH_3COO \cdot 3H_2O$. J Cryst Growth. 1990;99:72–6.

13. Wang XQ, Xu D, Lu MK, Yuan DR, Huang J, Li SG, Lu GW, Sun HQ, Guo SY, Zhang GH, Duan XL, Liu HY, Liu WL. Physicochemical behavior of nonlinear optical crystal $CdHg(SCN)_4$. J Cryst Growth. 2003;247:432–7.
14. Uthrakumar R, Vesta C, Justin Raj C, Dinakaran S, Christhu Dhas R, Jerome Das S. Optical and dielectric studies on pure and Ni^{2+}, Co^{2+} doped single crystals of bis thiourea cadmium chloride. Cryst Res Technol. 2008;43:428–32.
15. Rajasekaran R, Rajendiran KV, Mohan Kumar R, Jayavel R, Dhanasekaran R, Ramasamy P. Investigation on the nucleation kinetics of zinc thiourea chloride (ZTC) single crystals. Mater Chem Phys. 2003;82:273–80.
16. Rajasekaran R, Ushashree PM, Jayavel R, Ramasamy P. Growth and characterization of zinc thiourea chloride (ZTC): a semiorganic nonlinear optical crystal. J Cryst Growth. 2001;229:563–7.
17. Moitra S, Kar T. Growth, optical and thermal characterization of bis(thiourea)zinc chloride single crystals. Opt Mater. 2008;30: 1621–4.
18. Rajasekaran R, Mohankumar R, Jeyavel R, Ramasamy P. Influence of pH on the growth and characteristics of nonlinear optical zinc thiourea chloride (ZTC) single crystals. J Cryst Growth. 2003;252:317–27.
19. Kushwaha SK, Vijayan N, Bhagavannarayana G. Growth by SR method and characterization of bis(thiourea)zinc(II) chloride single crystals. Mater Lett. 2008;62:3931–3.
20. Uthrakumar R, Vesta C, Justin Raj C, Krishnan S, Jerome Das S. Bulk crystal growth and characterization of non-linear optical bisthiourea zinc chloride single crystal by unidirectional growth method. Curr Appl Phys. 2010;10:548–52.
21. Selvakumar S, Rajarajan K, RaviKumar SM, Vetha Potheher I, Prem Anand D, Ambujam K, Sagayaraj P. Growth and characterization of pure and metal doped bis(thiourea) zinc chloride single crystals. Cryst Res Technol. 2006;41:766–70.
22. Moitra S, Kar T. Synthesis and characterization of bis(thiourea)zinc chloride doped with L-arginine. Mater Chem Phys. 2009;117:204–8.
23. Balu T, Rajasekaran TR, Murugakoothan P. Nucleation studies of ZTC doped with L-arginine in supersaturated aqueous solutions. Phys B. 2009;404:813–1818.
24. Dhumane NR, Hussaini SS, Dongre VG, Ghugare P, Shirsat MD. Growth and characterization of L-alanine-doped zinc thiourea chloride single crystal (ZTC). Appl Phys A. 2009;95:727–32.
25. Nithya K, Karthikeyan B, Ramasamy G, Muthu K, Meenakshisundaram SP. Growth and characterization of Fe^{3+}-doped bis(thiourea)zinc(II) chloride crystals. Spectrochim Acta A. 2011; 79:1648–53.
26. Du YX, Sun Y, Chen WC, Chen XL, Zhang DF. Growth and electrical properties of Mg:α-$LiIO_3$ crystal. J Cryst Growth. 2006;291:424–7.
27. Selvakumar S, Rajasekar SA, Thamizharasan K, Sivanesan S, Ramanand A, Sagayaraj P. Thermal, dielectric and photoconductivity studies on pure, Mg^{2+} and Zn^{2+} doped BTCC single crystals. Mater Chem Phys. 2005;93:356–60.
28. Selvakumar S, Packiam Julius J, Rajasekar SA, Ramanand A, Sagayaraj P. Microhardness, FTIR and transmission spectral studies of Mg^{2+} and Zn^{2+} doped nonlinear optical BTCC single crystals. Mater Chem Phys. 2005;89:244–8.
29. Qiao H, Xu J, Tomita Y, Zhu D, Fu B, Zhang G, Zhang G. UV-light-induced one-color and two-color photorefractive effects in congruent and near-stoichiometric $LiNbO_3$:Mg crystals. Opt Mater. 2007;29:889–95.
30. Zhang T, Wang B, Zhao Y, Fang S, Ma D, Xu Y. Optical homogeneity and second harmonic generation in Li-rich Mg-doped $LiNbO_3$ crystals. Mater Chem Phys. 2004;88:97–101.
31. Sun X, Guo S, Wu G, Li M, Zhao X. The influence of Mg doping on the dielectric and tunable properties of $(Ba_{0.6}Sr_{0.4})_{0.925}K_{0.075}TiO_3$ thin films fabricated by sol–gel method. J Cryst Growth. 2006; 290:121–6.
32. Mojumdar SC, Raki L. Preparation, thermal, spectral and microscopic studies of calcium silicate hydrate-poly(acrylic acid) nanocomposite materials. J Therm Anal Calorim. 2006;85:99–105.
33. Sawant SY, Verenkar VMS, Mojumdar SC. Preparation, thermal, XRD, chemical and FT-IR spectral analysis of $NiMn_2O_4$ nanoparticles and respective precursor. J Therm Anal Calorim. 2007; 90:669–72.
34. Porob RA, Khan SZ, Mojumdar SC, Verenkar VMS. Synthesis, TG, SDC and infrared spectral study of $NiMn_2(C_4H_4O_4)_3 \cdot 6N_2H_4$—a precursor for $NiMn_2O_4$ nanoparticles. J Therm Anal Calorim. 2006;86:605–8.
35. Mojumdar SC, Varshney KG, Agrawal A. Hybrid fibrous ion exchange materials: past, present and future. Res J Chem Environ. 2006;10:89–103.
36. Doval M, Palou M, Mojumdar SC. Hydration behaviour of C_2S and C_2AS nanomaterials, synthesized by sol–gel method. J Therm Anal Calorim. 2006;86:595–9.
37. Mojumdar SC, Moresoli C, Simon LC, Legge RL. Edible wheat gluten (WG) protein films: preparation, thermal, mechanical and spectral properties. J Therm Anal Calorim. 2011;104:929–36.
38. Varshney G, Agrawal A, Mojumdar SC. Pyridine based cerium(IV) phosphate hybrid fibrous ion exchanger: synthesis, characterization and thermal behaviour. J Therm Anal Calorim. 2007;90:731–4.
39. Mojumdar SC, Melnik M, Jona E. Thermal and spectral properties of Mg(II) and Cu(II) complexes with heterocyclic *N*-donor ligands. J Anal Appl Pyrolysis. 2000;53:149–60.
40. Borah B, Wood JL. Complex hydrogen bonded cations. The benzimidazole benzimidazolium cation. Can J Chem. 1976;50: 2470–81.
41. Mojumdar SC, Sain M, Prasad RC, Sun L, Venart JES. Selected thermoanalytical methods and their applications from medicine to construction. J Therm Anal Calorim. 2007;60:653–62.
42. Meenakshisundarm SP, Parthiban S, Madhurambal G, Mojumdar SC. Effect of chelating agent (1,10-phenanthroline) on potassium hydrogen phthalate crystals. J Therm Anal Calorim. 2008;94:21–5.
43. Rejitha KS, Mathew S. Investigations on the thermal behavior of hexaamminenickel(II) sulphate using TG-MS and TR-XRD. Glob J Anal Chem. 2010;1(1):100–8.
44. Pajtášová M, Ondrušová D, Jóna E, Mojumdar SC, Ľalíková S, Bazyláková T, Gregor M. Spectral and thermal characteristics of copper(II) carboxylates with fatty acid chains and their benzothiazole adducts. J Therm Anal Calorim. 2010;100:769–77.
45. Madhurambal G, Ramasamy P, Anbusrinivasan P, Vasudevan G, Kavitha S, Mojumdar SC. Growth and characterization studies of 2-bromo-4′-chloro-acetophenone (BCAP) crystals. J Therm Anal Calorim. 2008;94:59–62.
46. Gonsalves LR, Mojumdar SC, Verenkar VMS. Synthesis and characterisation of $Co_{0.8}Zn_{0.2}Fe_2O_4$ nanoparticles. J Therm Anal Calorim. 2011;104:869–73.
47. Raileanu M, Todan L, Crisan M, Braileanu A, Rusu A, Bradu C, Carpov A, Zaharescu M. Sol–gel materials with pesticide delivery properties. J Environ Prot. 2010;1:302–13.
48. Varshney KG, Agrawal A, Mojumdar SC. Pectin based cerium(IV) and thorium(IV) phosphates as novel hybrid fibrous ion exchangers synthesis, characterization and thermal behaviour. J Therm Anal Calorim. 2005;81:183–9.
49. Mojumdar SC, Šimon P, Krutošíková A. [1]Benzofuro[3,2-c]pyridine: synthesis and coordination reactions. J Therm Anal Calorim. 2009;96:103–9.
50. Moricová K, Jóna E, Plško A, Mojumdar SC. Thermal stability of Li_2O–SiO_2–TiO_2 gels evaluated by the induction period of crystallization. J Therm Anal Calorim. 2010;100:817–20.

51. Mojumdar SC, Miklovic J, Krutosikova A, Valigura D, Stewart JM. Furopyridines and furopyridine-Ni(II) complexes—synthesis, thermal and spectral characterization. J Therm Anal Calorim. 2005;81:211–5.
52. Vasudevan G, Anbu Srinivasan P, Madhurambal G, Mojumdar SC. Thermal analysis, effect of dopants, spectral characterisation and growth aspects of KAP crystals. J Therm Anal Calorim. 2009;96:99–102.
53. Lal K, Bhagavannarayan G. A high-resolution diffuse X-ray scattering study of defects in dislocation-free silicon crystals growth by the float-zone method and comparison with Czochralski-grown crystals. J Appl Cryst. 1989;22:209–15.
54. Batterman BW, Cole H. Dynamical diffraction of X-rays by perfect crystals. Rev Mod Phys. 1964;36:681–717.
55. Albert Cotton F, Wilkinson G. Advanced inorganic chemistry. Second ed. New Delhi: Wiley Eastern Limited; 1970. p. 45.